# Preparation of Hexagonal-Boron Nitride Nanoparticles by Laser Ablation in Liquid and their Properties

Kazuki Yamada, Yoshitaka Kitamoto, and Hiroyuki Wada*

*School of Materials and Chemical Technology, Tokyo Institute of Technology, Japan*
**Corresponding author's e-mail: wada.h.ac@m.titech.ac.jp*

Hexagonal boron nitride nanoparticles were successfully prepared by laser ablation in liquid. A nanosecond laser at the second harmonic of Nd:YAG was used for the preparation, and they were evaluated by scanning electron microscopy, X-ray diffraction, and dynamic light scattering. Increasing the laser fluence reduced the secondary particle size, yielding particles of 379 nm. The high-temperature laser process did not cause any phase change, and hexagonal boron nitride nanoparticles were obtained. Decreasing the amount of sodium hydroxide solution added to the solvent of laser ablation reduced the amount of agglomeration and reduced the secondary particle size, yielding nanoparticles of 189 nm. The zeta potential of the prepared nanoparticle was -62 mV and the primary particle diameter was 25 nm.

DOI: 10.2961/jlmn.2023.03.2006
**Keywords:** laser ablation, nanomaterial, nitride, crystal structure

## 1. Introduction

Boron nitride (BN) has a structure very similar to that of carbon materials and has attracted attention due to its unique properties.[1)] BN has two main crystal structures: hexagonal-BN, which is stable in the ambient phase, and cubic-BN, which is stable in the high-pressure phase.[2)] Hexagonal-BN has a graphene-type structure with planar hexagonal rings consisting of alternating bonds of B and N. In the case of graphene, the hexagonal rings of only carbon are stacked vertically, but in the case of BN, N is below B and B is below N alternately.[3)] While graphene has no band gap, hexagonal-BN is an insulator with a band gap as large as about 6 eV.[3)]

BN nanoparticles are very useful for specific application potentials in catalysis, drug delivery, tribology, and structural materials.[1)] They are widely used as support materials for catalysts due to their large specific surface area and high chemical stability.[1)] Hexagonal BN is useful as a catalyst and photocatalyst due to its unique electronic structure.[4-7)] BN nanoparticles have been used as drug delivery systems of ciprofloxacin (CIP),[8)] norfloxacin (NOR),[8)] and doxorubicin (DOX).[9,10)] H-BN nanoparticles are also important in the field of tribology and are widely known as additives to oils, solid lubricants, etc.[11)] Embedding BN nanoparticles in polymers has enabled composite materials with lightweight and high mechanical strength, and given them low thermal expansion coefficient and high thermal conductivity properties.[12,13)]

Nanoparticles in themselves have an extremely large specific surface area and exhibit properties different from those of the bulk, making them suitable for various applications such as catalysts, biomaterials, and electronic materials. Nanoparticles can be prepared by hydrothermal synthesis,[14)] solvothermal synthesis,[15)] chemical bath deposition,[16)] pyrolysis,[17)] sol-gel method,[18)] and laser ablation in liquid.[19,20)] The laser ablation in liquid method has recently attracted attention as a new nanoparticle fabrication method, which proceeds as follows:[21-23)] i) A brief interaction between a pulsed laser beam and a solid target would result in the formation of an atomic plasma on the target surface after a few nanoseconds. ii) The plasma would generate by the high-velocity expansion of the material exposed to the high-energy laser beam would reach a high temperature and pressure, generating a shock wave in the surrounding area. iii) The energy released from the hot plasma into the surrounding liquid would cool the liquid, causing a thin vapor layer to appear around the plasma volume, which would be the beginning of the rise of the cavitation bubble. iv) Finally, the formation of nanoparticles would occur during the cooling phase of the plasma and would diffuse into the liquid during the contraction phase of the cavitation bubble, which would lead to the formation of a colloidal solution. The advantages of the laser ablation in liquid are as follows; (i) Nanoparticles with high crystallinity can be obtained due to the high temperature and pressure conditions. (ii) The collection rate is high because all the generated nanoparticles are present in the liquid. (iii) The generated nanoparticles are obtained as colloids, making them easy to handle. (iv) The size and shape of the nanoparticles can be controlled by changing the laser conditions. (v) No vacuum equipment is required, and nanoparticles can be produced with simple equipment.

It had been reported that laser ablation in liquid with electrolytes such as sodium chloride, potassium chloride, sodium hydroxide, hydrochloric acid, and sodium nitrate increased the surface charge density and electrostatic stability of nanoparticles.[24)] Metal nanoparticles produced with electrolyte solution showed not only a decrease in particle size but also an improvement in dispersion stability due to the hydroxide and chloride ions adsorbed on the particle surface.[25)] In palladium nanoparticles, higher colloidal stability and monodisperse nanoparticles were obtained by adsorption of anions, and laser ablation using electrolytes with tailored ionic strength was reported to be a promising approach for controlling colloidal stability and particle size.[26)]

In this study, hexagonal-BN nanoparticles are prepared by dispersing BN micron-size powder in pure water or electrolytic solution and irradiating them with a laser, and their properties were characterized after laser irradiation. By performing laser ablation in liquid with the electrolytic solution, ions are expected to adsorb on the surface of BN nanoparticles and form BN nanoparticles with improved size control and dispersion stability through electrostatic repulsion.

## 2. Experimental

A suspension of hexagonal-BN powder (particle size: 10 μm, purity: >99.0%) was weighed into a screw-tube bottle (30 ml), added to which ultrapure water (20 ml) was added, stirred for 30 sec. with a vortex mixer, and irradiated with ultrasound for 5 min. The nanoparticles were prepared by irradiating the suspension with Nd:YAG laser beam (wavelength: 532 nm, pulse width: 13 ns, repetition rate: 10 Hz). During laser irradiation, the powder was dispersed by a magnetic stirrer. After laser irradiation, the sample was passed through a 1 μm filter to obtain the nanoparticle dispersion solution.

Samples were observed by scanning electron microscope (SEM, acceleration voltage: 5 kV) to evaluate the shape and primary particle size of the nanoparticles. The sample was prepared by dropping 2.5 μl onto a carbon support film on a metal mesh and allowing it to dry. Powder X-ray diffraction (XRD, power: 40 kV, 40 mA) was used to evaluate the crystal structure of the samples. The samples were powdered from nanoparticle-dispersed solution using a freeze-dry. The secondary particle size of the prepared nanoparticles was measured by dynamic light scattering (DLS, light source wavelength: 532 nm, detection angle: 90 deg.). Three ml of the prepared nanoparticle dispersion was placed in a cell for the measurement. The zeta potential of the prepared nanoparticles was measured by the electrophoretic laser Doppler method. The laser Doppler method is based on the fact that the frequency of scattered light changes due to the Doppler effect when particles moving by electrolysis are irradiated with laser light, and the zeta potential can be measured in a short time.

## 3. Results and Discussion

Figure 1 shows SEM images of the raw material and the nanoparticles produced by varying the fluence with an irradiation time of 30 minutes. The raw material was a plate-like particle of micrometer order, as shown in Fig. 1(a). At a fluence of 75 mJ/cm$^2$, nanoparticles could also be observed, although in smaller numbers, as shown in Fig. 1(b). A large number of micro-sized particles were also observed. In the case of fluences of 150 and 300 mJ/cm$^2$, aggregated nanoparticles were mainly observed, as shown in Fig. 1(c) and (d). The formation mechanism of BN nanoparticles would be due to the growth and collapse of cavitation bubbles caused by the heating of the raw material powders by the laser beam. It would be as follows;[27] When the raw material powders were irradiated with the laser beam, the plasma would be generated on the surface of the powders. The expanding plasma plume contained ions, atomic clusters, and fine particles. A shock wave would be generated then. The plasma plume would be cooled as it expanded, releasing energy into the liquid. Cavitation bubbles would be generated during this process, and the cavitation bubbles would expand, contract, and collapse repeatedly to produce nanoparticles. This process would be followed by particle growth and aggregation. There are many reports on the relationship between cavitation bubbles and nanoparticle formation.[28-31] A large amount of agglomeration of nanoparticles in Fig. 1(c) and (d) would be due to the increase in the number of nanoparticles produced by the increase in laser fluence.[32] Nanoparticles are likely to aggregate due to their extremely high

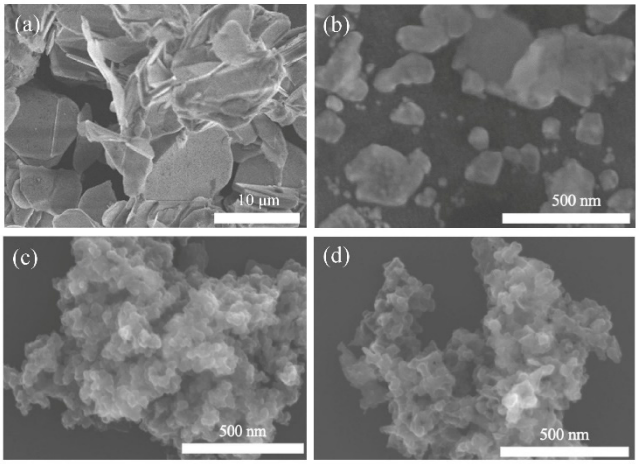


**Fig. 1** SEM images of (a) raw material and nanoparticles at each fluence ((b) 75 mJ/cm$^2$, (c) 150 mJ/cm$^2$ and (d) 300 mJ/cm$^2$).

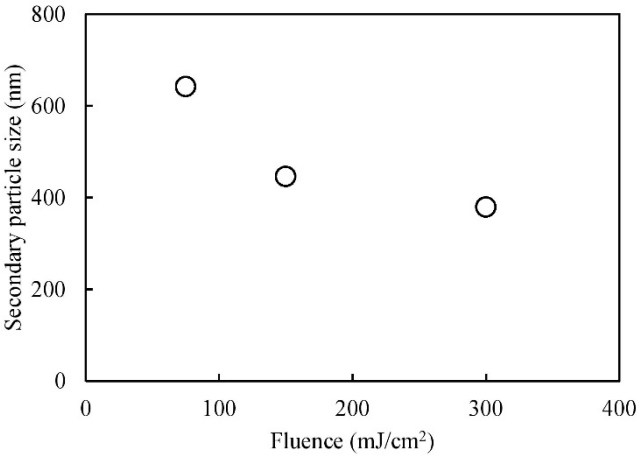


**Fig. 2** The average secondary particle size of nanoparticles as a function of irradiation-laser fluence.

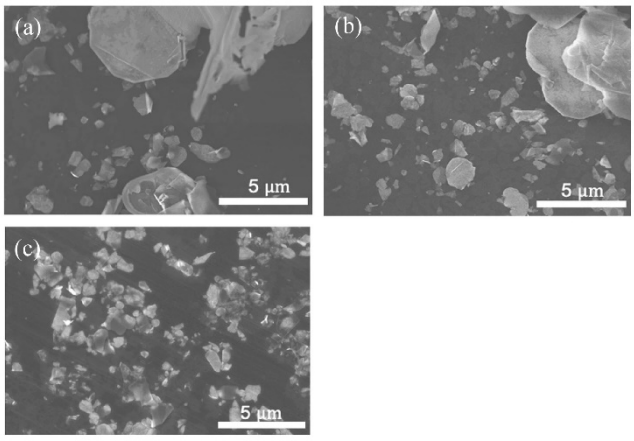


**Fig. 3** SEM images of nanoparticles at each irradiation time ((a) 0.5 hours, (b) 1.0 hour and (c) 1.5 hours).

surface energy.[33] In addition, nanoparticles in water would be constantly moving due to flow and diffusion caused by Brownian motion, therefore when there was a relative velocity difference between particles, they would collide with each other, and if the gravitational force acting between the nanoparticles during this collision would be sufficiently large, they would agglomerate.[34]

The fluence dependence of the average secondary particle size measured by DLS is shown in Figure 2. Particle size decreased with increasing laser fluence. A similar trend had been observed for other materials.[35-38]

Figure 3 shows the SEM images when the laser irradiation time was extended to reduce agglomerates. The number of fine particles increased as the irradiation time increased. Although the BN raw material powder dispersion was continuously stirred by the magnetic stirrer during the laser irradiation, some particles would not be irradiated by the laser beam if the irradiation time was small. By increasing the irradiation time, the number of powders irradiated with the laser beam increased, and it would increase the number of nanoparticles. According to the photothermal mechanism,[39,40] which was one of the mechanisms of nanoparticle formation by laser irradiation, the particle temperature would increase by Joule heating with increasing laser fluence and irradiation time, and explosive evaporation would occur at the boiling point to produce nanoparticles. In this study, the increase in irradiation time would also cause the progression of fragmentation of powders.

Figure 4 shows the XRD patterns of the raw material and nanoparticles. Both were all hexagonal-BN peaks, and no cubic-BN peaks were observed, so no phase change was observed under the present conditions, even with the high-temperature laser process.

The dependence of the secondary particle size of the nanoparticles on electrolyte concentration in the case of KCl solution is shown in Figure 5. The secondary particle diameter in the case of ultrapure water was 296.4 nm. At all concentrations, the secondary particle diameters were larger than those in the case of ultrapure water and also increased with increasing concentration. For an interface that is positively or negatively charged in the electrolyte, ions of opposite charge are distributed to neutralize it.[41,42] The potential $\varphi$ at a distance d from the interface is expressed by the following equation (1);[41,42]

$$\varphi = \varphi_\delta e^{-\kappa d} \qquad (1)$$

where $\varphi\delta$ is the potential of the Stern layer fixed at the interface, and $\kappa$ is the reciprocal of the thickness of the electric double layer when $\varphi$ is $1/e$ of $\varphi\delta$. $\kappa$ is expressed by the following equation (2);[41,42]

$$\kappa = \left(\frac{8\pi z^2 e^2 n}{\varepsilon k T}\right)^{1/2} \qquad (2)$$

where $z$ is ionic valence, $e$ is elementary electric charge, $n$ is ionic concentration, $\varepsilon$ is dielectric constant, $k$ is Boltzmann's constant, and $T$ is the absolute temperature. As the ionic concentration increases, the thickness of the electric double layer decreases, the repulsion due to surface charges decreases, and aggregation of nanoparticles occurs. In DLVO theory, the height of the barrier is determined by the conditions under which the particles exist, with agglomeration occurring in systems with low barriers and remaining dispersed in systems with high barriers.[41,42] The increase in the

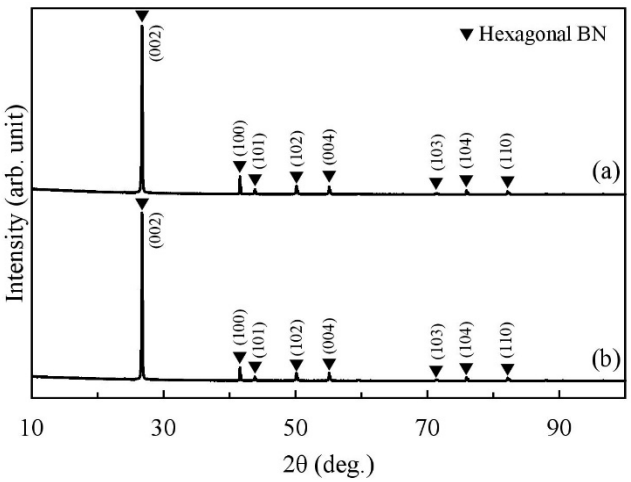


**Fig. 4** XRD spectra of (a) raw material and (b) nanoparticles (Laser fluence: 300 mJ/cm$^2$, irradiation time: 1.5 hours).

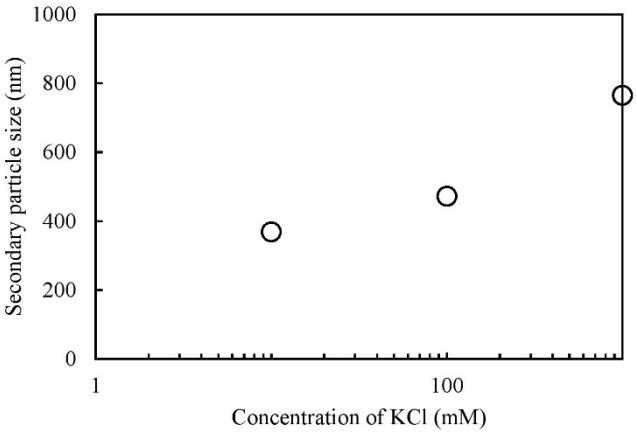


**Fig. 5** The average secondary particle size of nanoparticles as a function of the concentration of KCl.

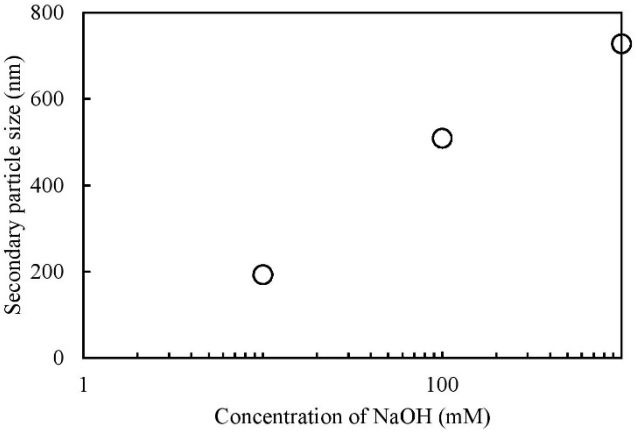


**Fig. 6** The average secondary particle size of nanoparticles as a function of the concentration of NaOH.

electrolyte concentration in this experiment would decrease the electric double-layer repulsion between nanoparticles and increase the aggregation rate. The increase in KCl concentration also caused aggregation because the pH was closer to the zero-point charge of BN.[43]

Figure 6 indicates the dependence of secondary particle size on electrolyte concentration in the case of NaOH solution. As the electrolyte concentration decreased, the secondary particle size decreased, and at 10 mM it was smaller than

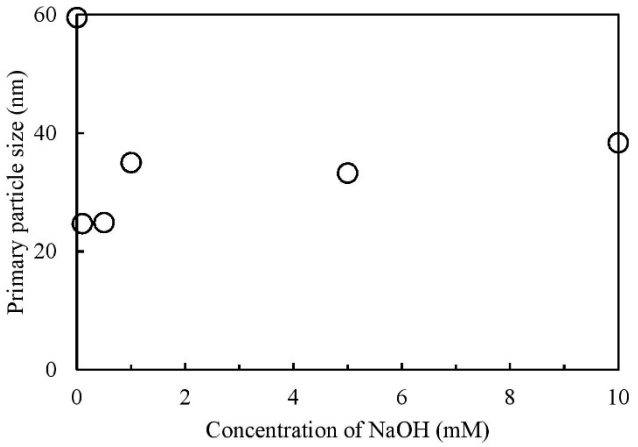


**Fig. 7** The average primary particle size of nanoparticles as a function of the concentration of NaOH at low concentration.

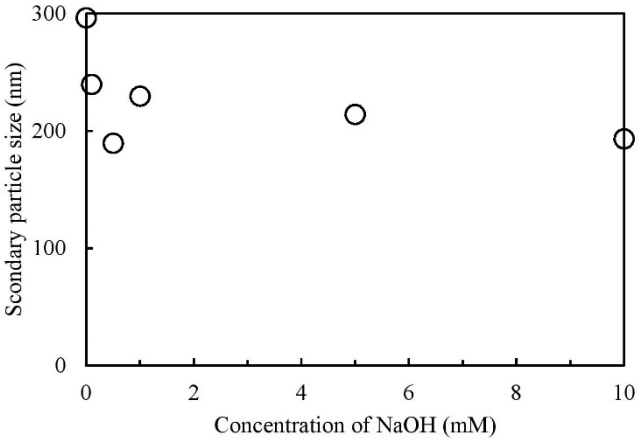


**Fig. 8** The average secondary particle size of nanoparticles as a function of concentration of NaOH at low concentration.

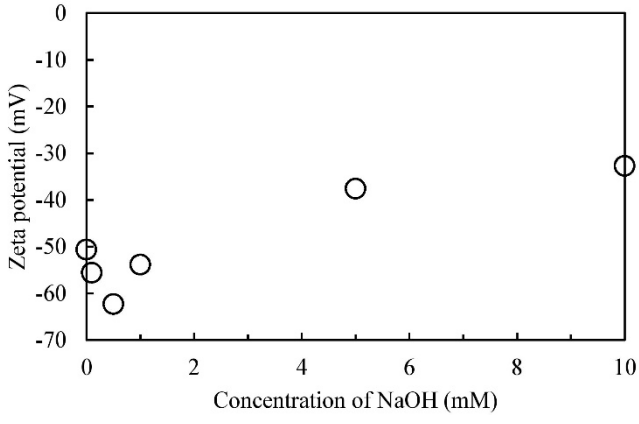


**Fig. 9** Zeta potential of nanoparticles as a function of concentration of NaOH at low concentration.

that in ultrapure water. It would be due to the increase in repulsion between nanoparticles by the electric double layer and the suppression of agglomeration as the electrolyte concentration decreased. In the case of BN, the zero-point charge of which is 4.3,[43] nanoparticles are dispersed by electrostatic repulsion when the pH is far from the isoelectric point, which means a strongly alkaline solution. KCl is neutral, whereas NaOH is an alkaline solution. Therefore, the nanoparticles in NaOH were dispersed more.

Figure 7 shows the primary particle size measured by SEM for each NaOH concentration below 10 mM. All NaOH concentrations showed smaller primary particle diameters than in ultrapure water. It was smallest at NaOH concentrations of 0.1 mM and 0.5 mM. In a previous study, it was reported that in the generation of ZnO nanoparticles by laser ablation in liquid with NaOH solution, smaller nanoparticles were obtained than those prepared with deionized water.[44] In this study, it was also suggested that the presence of a base would suppress the growth of nanoparticles.

Figure 8 shows the secondary particle diameters at each NaOH concentration. At all concentrations, the secondary particle diameters were smaller than those obtained with ultrapure water. Hydroxide ions would adsorb on the nanoparticle surfaces and the electrostatic repulsion between the nanoparticles would increase, which suppressed aggregation.[45] The secondary particle size decreased gradually with increasing electrolyte concentration, but a sharp decrease was observed around 0.5 mM. The tendency would be related to the sharp decrease around 0.5 mM in Figure 7.

Figure 9 shows the zeta potential at each NaOH concentration. The absolute value of the potential decreased at concentrations above 0.5 mM. From Eq. 2, the thickness of the electric double layer is given by the reciprocal of $\kappa$ and decreases with increasing electrolyte concentration $n$. Above 0.5 mM, the electric double layer was compressed as the concentration increased, and thus the zeta potential decreased.[41,42]

## 4. Conclusions

Hexagonal-BN nanoparticles were prepared by laser ablation in liquid and characterized. The secondary particle size was reduced by increasing the laser fluence. The number of nanoparticles was increased by increasing the irradiation time. The addition of 0.5 mM low-concentration sodium hydroxide further reduced primary and secondary particle size.

## Acknowledgments

The authors wish to thank K. Nakamura at Tokyo Tech. This study was supported by JSPS KAKENHI Grant, and Open Facility Center (Tokyo Tech.).

## References

[1] D.V. Shtansky, K.L. Firesteinb, and D.V. Golberg: Nanoscale, 10, (2018) 17477.
[2] V.L. Solozhenko: High Pressure Res., 13, (1995) 199.
[3] A. Janotti, S.-H. Wei, and D.J. Singh: Phys. Rev. B, 64, (2001) 174107.
[4] K. Uosaki, G. Elumalai, H. Noguchi, T. Masuda, A. Lyalin, A. Nakayama, and T. Taketsugu: J. Am. Chem. Soc., 136, (2014) 6542.
[5] D. Xu, Y.-J. Liu, J.-X. Zhao, Q.-H. Cai, and X.-Z. Wang: J. Phys. Chem. C, 118, (2014) 8868.
[6] S. Lin, J. Huang, and X. Ye: Appl. Surf. Sci., 320, (2014) 237.
[7] Y. Song, H. Xu, C. Wang, J. Chen, J. Yan, Y. Xu, Y. Li, C. Liu, H. Li, and Y. Lei: RSC Adv., 4, (2014) 56853.

[8] P. Singla, N. Goel, and S. Singhal: Chem. Eng. J., 299, (2016) 403.
[9] I.V. Sukhorukova, I.V. Zhitnyak, A.M. Kovalskii, A.T. Matveev, O.I. Lebedev, N.A. Gloushankova, X. Li, D. Golberg, and D.V. Shtansky: ACS Appl. Mater. Interfaces, 7, (2015) 17217.
[10] I.Y. Zhitnyak, I.N. Bychkov, I.V. Sukhorukova, A.M. Kovalskii, K.L. Firestein, D. Golberg, N.A. Gloushankova, and D.V. Shtansky: ACS Appl. Mater. Interfaces, 9, (2017) 32498.
[11] M.S. Charoo and M.F. Wani: Lubr. Sci., 29, (2017) 241.
[12] Y.K. Kim, J.Y. Chung, J.G. Lee, Y.K. Baek, and P.W. Shin: Composites Part A, 98, (2017) 184.
[13] Chunli Zhang, Yi He, Fei Li, Haihui Di, Lei Zhang, and Yingqing Zhan: J. Alloys Compd., 685, (2016) 743.
[14] M. Salavati-Niasari, S. Alizadeh, M. Mousavi-Kamazani, N. Mir, O. Rezaei, and E. Ahmadi: J. Clust. Sci., 24, (2013) 1181.
[15] K.J. Huang, J.Z. Zhang, and Y. Fan: J. Alloys Compd., 625, (2015) 158.
[16] M. Xin, K. Li, and H. Wang: Appl. Surf. Sci., 256, (2009) 1436.
[17] F. Davar, M.R. Loghman-Estarki, M. Salavati-Niasari, and M. Mazaheri: J. Clust. Sci., 27, (2016) 593.
[18] F. Selim, A. Khamehchi, D. Winarski, and S. Agarwal: Opt. Mater. Express, 6, (2016) 3704.
[19] J. Neddersen, G. Chumanov, and T. Cotton: Appl. Spectrosc., 47, (1993) 1959.
[20] A. Fojtik and A. Henglein: Ber. Bunsen Ges. Phys. Chem. Chem. Phys., 97, (1993) 252.
[21] Tatiana E. Itina: J. Phys. Chem. C, 115, (2011) 5044.
[22] Kohichi Hirata, Satoru Masai, Tetsuo Sakka, and Yukio H. Ogata: Proc. of SPIE, 5713, (2005) 311.
[23] Afifa Riahi, Saleh Khamlich, Moncef Balghouthi, Touria Khamliche, Terence Brian Doyle, Wissem Dimassi, Amenallah Guizani, and Malik Maaza: J. Mol. Liq., 304, (2020) 11.
[24] Pattarin Chewchinda, Osamu Odawara, and Hiroyuki Wada: CheM, 2016, (2016) 1.
[25] Christoph Rehbock, Vivian Merk, Lisa Gamrad, René Streubel, and Stephan Barcikowski: Phys. Chem. Chem. Phys., 15, (2013) 3057.
[26] Galina Marzun, Junji Nakamura, Xiaorui Zhang, Stephan Barcikowski, and Philipp Wagener: Appl. Surf. Sci., 348, (2015) 75.
[27] S. Hashimoto: Rev. Laser Eng., 45, (2017) 257.
[28] N. Takada, T. Nakano, and K. Sasaki: Appl. Surf. Sci., 255, (2010) 9572.
[29] Wafaa Soliman, Noriharu Takada, and Koichi Sasaki: Appl. Phys. Express, 3, (2010) 035201.
[30] Wafaa Soliman, Tetsutaro Nakano, Noriharu Takada, and Koichi Sasaki, Jpn. J. Appl. Phys., 49, (2010) 116202.
[31] Koichi Sasaki and Noriharu Takada: Pure Appl. Chem., 82, (2010) 1317.
[32] Hiroki Kobayashi, Pattarin Chewchinda, and Hiroyuki Ohtani, Osamu Odawara, and Hiroyuki Wada: J. Phys. Conf. Ser., 441, (2013) 012035.
[33] S. Umar, F. Sulaiman, N. Abdullah, and S. N. Mohamad: Proc. 3rd Int. Sci. Technol. Eng. Conf. (ISTEC) 2018 Mater. Chem., 2031, (2018) 020031.
[34] L. Feng and Y. Adachi: Colloids and Surfaces A: Physicochem. Eng. Aspects, 454, (2014) 128.
[35] Kazuki Isoda, Ryuga Yanagihara, Yoshitaka Kitamoto, Masahiko Hara, and Hiroyuki Wada: IEICE Trans. Electronics, E104-C, (2021) 390.
[36] Teruki Akimori, Kentaro Nakamura, Tsuyoshi Asahi, and Hiroyuki Wada: J. Laser Appl., 32, (2020) 022070.
[37] Keita Omura, Ryuga Yanagihara, and Hiroyuki Wada: Jpn. J. Appl. Phys., 58, (2019) 128002.
[38] Ryuga Yanagihara, Tsuyoshi Asahi, Yukihide Ishibashi, Osamu Odawara, and Hiroyuki Wada: Jpn. J. Appl. Phys., 57, (2018) 035001.
[39] A. Takami, H. Kurita, and S. Koda: J. Phys. Chem. C, 111, (1999) 11246.
[40] S. Inasawa, M. Sugiyama, and Y. Yamaguchi: J. Phys. Chem. B, 109, (2005) 9404.
[41] B.V. Derjaguin and L.D. Landau: Acta Physicochim, 14, (1941) 633.
[42] E.J. Verwey and J.Th.G. Overbeek: Theory of Stability of Lyophobic Colloid, Elsevier, Amsterdam (1948).
[43] R.H. Yoon, T. Salman, and G. Donnay: J. Colloid Interface Sci., 70, (1979) 483.
[44] Chun He, Takeshi Sasaki, Hiroyuki Usui, Yoshiki Shimizu, and Naoto Koshizaki: J. Photochem. Photobiol. A, 191, (2007) 66.
[45] Galina Marzun, Junji Nakamura, Xiaorui Zhang, Stephan Barcikowski, and Philipp Wagener: Appl. Surf. Sci., 348, (2015) 75.

(Received: June 15, 2023, Accepted: October 12, 2023)